Etched Graphite with Internally Grown Si Nanowires from Pores as an Anode for High Density Li-Ion Batteries

Sookyung Jeong, Jung-Pil Lee, Minseong Ko, Guntae Kim, Soojin Park,* and Jaephil Cho*

Interdisciplinary School of Green Energy, Ulsan National Institute of Science and Technology (UNIST), Ulsan 689-798, South Korea

ⓢ Supporting Information

ABSTRACT: A novel architecture consisting of Si nanowires internally grown from porous graphite is synthesized by etching of graphite with a lamellar structure via a VLS (vapor–liquid–solid) process. This strategy gives the high electrode density of 1.5 g/cm^3, which is comparable with practical anode of the Li-ion battery. Our product demonstrates a high volumetric capacity density of 1363 mAh/cm^3 with 91% Coulombic efficiency and high rate capability of 568 mAh/cm^3 even at a 5C rate. This good electrochemical performance allows porous graphite to offer free space to accommodate the volume change of Si nanowires during cycling and the electron transport to efficiently be improved between active materials.

KEYWORDS: Etched graphite, Si nanowires, Li-ion battery, electrode density, capacity retention
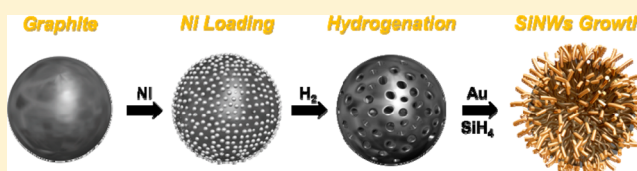
Nowdays, to meet the requirements for usages in hybrid electric vehicles (HEVs) and plug-in hybrid electric vehicles (PHEVs) as well as high energy storage system, the increasing energy density has been a key issue in rechargeable lithium ion batteries.[1,2] Currently available commercial Li-ion cells (~150 Wh/kg based on the mass of the battery pack) consisting of LiCoO$_2$ and graphite as the cathode and anode, respectively, cannot meet with the electrically powered applications which require a higher cell operating voltage and/or capacity.[3,4] On the cathode side, for example, although the surface chemistry plays a key role of solving an intrinsic problem such as capacity fade, the available capacity of Li$_x$MO$_2$ (M = transition metal) is limited to <180 mAh/g with a cutoff voltage of 4.3 V.[2,5]

To be concomitant with increasing the capacity of cathode materials, the alternative high capacity anode materials instead of graphite (372 mAh/g) should be considered to balance the cell. Among various kinds of anode candidates, silicon (Si) has been intensively paid attention to the alternative material to achieve high gravimetric capacity, 3579 mAh/g for Li$_{15}$Si$_4$ at room temperature (RT). However, despite its capacity merit, it has a severe drawback, that is, large expansion and contraction during cycling (Si + xLi$^+$ + xe$^-$ ↔ Li$_x$Si).[6-9] This volume change (>300% at RT) leads to pulverization, resulting in contact loss between current collector and carbon black and active particles. This loss eventually resulted in a significant capacity loss during cycling.

To circumvent this problem, various nanoengineering strategies have been proposed to minimize the volume-related problems using Si nanoparticles,[10] yolk-shell Si nanoparticle-amorphous carbon structure,[11] Si nanoparticles in nitrogen-doped carbon sphere,[12] Si nanowires,[13] carbon nanofiber coated Si nanowires,[14] Si nanotubes,[15] 3D porous Si nano-particles,[16] and porous Si−C composites.[17] Although these strategies exhibited very high capacity and good cycle stability, considering the very low of electrode density (<0.9 g/cm^3) of Si upon fully lithiation, the composite with graphite (1.7 g/cm^3) is the most efficient way to reach high energy density.

In this regard, physical blending of graphite and Si (also see Table S1) have been widely considered to produce Si/graphite composites, but these methods led to a capacity decrease during cycling due to the contact loss between electrode materials.[18,19] Also, the chemically bridged Si/graphite composite with a phenyl group was reported to overcome a capacity fading, but it also showed a rapid capacity fading from 1052 mAh/g at second cycle to 540 mAh/g at the 50th cycle with a capacity retention of 52%.[20] Here, it should be noted that no previous similar works related to internally Si NWs grown from the etched graphite particles have been reported to not only accommodate the volume change but also increase electrode density.

Herein, we report a novel architecture consisting of Si nanowires internally grown from pores in the etched graphite particles (namely, SiNWs-PG) with a high electrode density of 1.5 g/cm^3. These novel composites demonstrate a high volumetric capacity density of 1363 mAh/cm^3 with 91% Coulomb efficiency and high rate capability of 568 mAh/cm^3 at a 5C rate. One of the uniqueness of these composites is that porous graphite structure can offer free space to accommodate the volume change of internal embedded Si nanowires and provide a fast electron transfer pathway between graphite and Si, resulting in the improved electrochemical performance.

Figure 1 shows a schematic view and morphology of the synthesis process of SiNWs-PG (see also Figure S1). First,
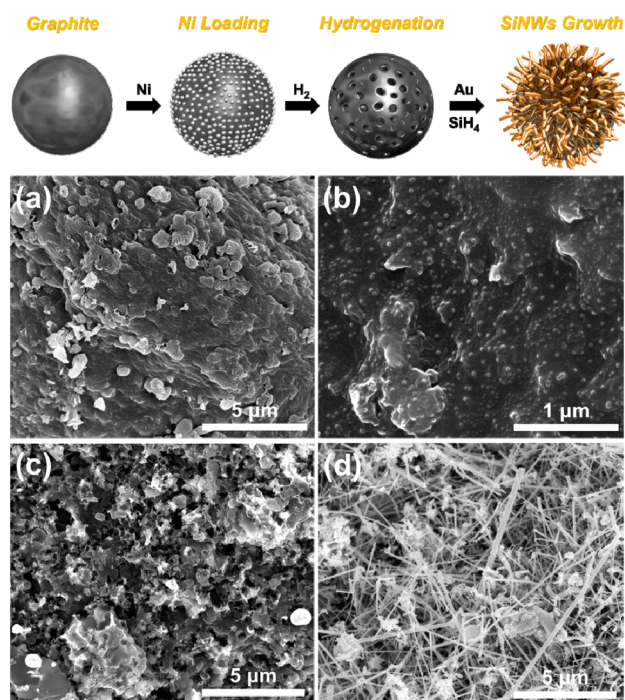
Figure 1. Top: Schematic view for the synthesis process of Si nanowires internally grown in porous graphite. Bottom: SEM images of (a) bare graphite, (b) loaded polystyrene-*b*-poly(2-vinylpyridine) micelles bearing Ni ion on graphite surface, (c) porous graphite after hydrogenation at 1000 °C for 1 h, and (d) Si nanowires grown from porous graphite after catalyst exchange from Ni to Au, followed by VLS process using SiH$_4$ at 550 °C for 30 min (for low magnification images, see Figure S1).

spherical micelles bearing Ni ions on graphite (∼20 μm diameter) were prepared by the selective complex formation of Ni ions and pyridine unit in a polystyrene-*b*-poly(2-vinyl-pyridine) (PS-*b*-P2VP) block copolymer. The micelle formation was induced by the difference in solubility between PS and Ni ion bearing P2VP in a selective solvent for PS, in which spherical micelles consisting of PS corona and P2VP core were formed in solution.[21] The micelles containing Ni ions were then transformed to self-assembled Ni nanoparticles after removal of polymer by heat treatment at 500 °C, followed by etching process in hydrogen atmosphere at 1000 °C for 1 h.[22] As a final step, Si nanowires were grown in 3D-interconnected pores of graphite particles via VLS process after exchange of catalyst from Ni to Au. The morphology of porous graphite and internally grown SiNWs was characterized by scanning electron microscopy (SEM). The Ni ion containing micelles deposited uniformly with a size of 30−40 nm on the graphite particle surface can be observed (Figure 1b). The as-prepared samples were annealed at 500 °C for 20 min to form Ni nanoparticles. Note that the catalytic gasification of carbon, called the etching process, is more favorable at the edge plane rather than the basal plane of graphene.[22] Therefore, microcarbon microbeads (MCMB) with the lamellar structure were used as a graphite source.[23] At 1000 °C, Ni nanoparticles on the graphite surface etch the edge plane via catalytic hydrogenation reaction (Ni + C$_{graphite}$ + 2H$_2$ → Ni + CH$_4$), where carbon atoms are absorbed into the Ni nanoparticles by carbon dissociation from graphene edge, resulting in a formation of porous structures with the remaining Ni nanoparticles (Figure 1c). As a result of etching process, graphite loses up to 20% of its original weight, and

pore sizes ranging from 200 nm to 1 μm were obtained, whereas the specific surface area was increased to 6.5 m^2/g compared to the bare sample (1.2 m^2/g). The cross-sectioned images obtained from a focused ion beam (cutting region with 6 μm of particle radius; Figure S2) showed the pores developed inside MCMB prepared by hydrogenation accompanying nickel penetration. As a second step, Si NWs in a scalable manner were grown in the porous graphite via the VLS process. In the VLS process, the catalyst plays an important constituent to serves as a preferential site for crystal nucleation and growth. If porous graphite with residual nickel is exposed at above the Ni−Si eutectic temperature,[24] Si nanowires can be expected to grow from the inside pores by SiH$_4$ gas decomposition. Upon annealing at 1200 °C, the nanowires were starting to grow. However, X-ray diffraction (XRD) patterns revealed that silicon carbide (SiC) was formed with Ni−Si alloy as liquid droplet on the tip of the nanowires (Figure S3). As a consequence, lower annealing temperatures are required to prevent SiC formation; therefore, Ni catalyst is needed to replace with Au because the eutectic point of Au−Si alloy can suppress SiC product. Considering the standard reduction potential between nickel and gold, Ni was dissolved in 1 mM HAuCl$_4$·H$_2$O solution via a galvanic displacement reaction, and Au was deposited on the porous graphite at the same time. After exchanging a catalyst, porous graphite with Au were annealed at 550 °C under SiH$_4$ flowing with 25 sccm for growing Si nanowires. As can be seen from SEM images in Figure 1d, Si nanowires are grown from porous graphite. In the controlled experiment (SiH$_4$ flow with 15 sccm at 550 °C for 30 min) to observe the evidence for the Si NWs grown from the pores in the etched graphite (Figure S3a and b), it can be clearly seen that Si nanowires are well grown from the pores. TEM results revealed that the catalyst are clearly shown on the top of Si nanowires and crystalline Si nanowires in SiNWs-PG is covered with 1−2 nm amorphous SiO$_2$ which is naturally produced after air exposure (Figure S4c and d).

To understand the variation of graphite structure after the hydrogenation process, it is characterized by XRD and Raman spectroscopy. Figure 2a shows a comparison of XRD patterns between bare and porous graphite. Note that the intensity ratio of (002) to (110) peaks at 26.4°, 77.4°, respectively, is indicative of the orientation degree of graphitic layers. Bare graphite has the value of 120.2 while the hydrogenated sample has the value of 46.5, which means that graphitic layers in porous graphite are less oriented with the more exposure of edge planes.[25] Also, Raman spectra (Figure 2b) display two major peaks at ∼1350 cm^{-1} and ∼1580 cm^{-1}, which are assigned to the D band and G band, respectively. In general, the D band is related to a breathing mode of A_{1g} symmetry, and this peak is not shown in perfect graphite structure. It becomes only active if the structure has the presence of disorder. Also, the G band is attributed to E_{2g} symmetry, which is associated with the in-plane bond stretching of sp^2 hybridized carbons.[26] The I_D/I_G ratio of porous graphite is 1.69 compared to bare graphite, 0.55, indicating that the disordered structure of sp^2 carbon is well-developed in porous graphite. Also, this result is consistent with SEM image (Figure 1c), showing that the edge planes are highly exposed with many pores. After the exchange of catalyst exchange, and followed by Si nanowire growth, the final product is predominantly composed of crystalline Si without showing Ni and SiC, as confirmed in Figure 2c. C1s region in XPS spectra is deconvoluted into three peaks at 284.1, 284.8, and 285.1 eV, which correspond to Si−C, C in graphite, and
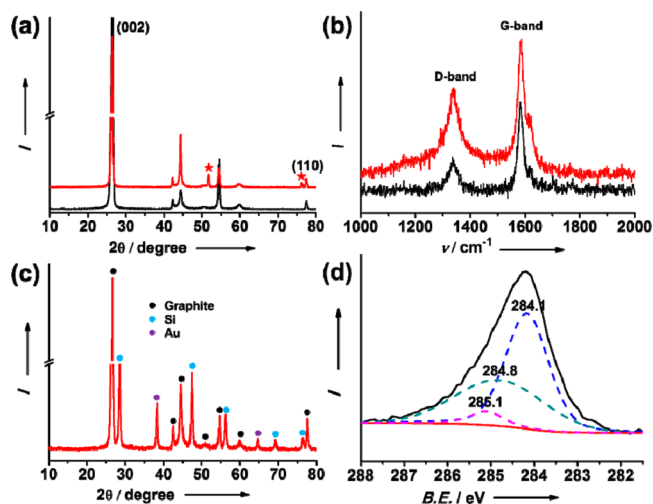
Figure 2. (a and b) XRD patterns (asterisks: Ni nanoparticles) and Raman spectra of bare graphite and porous graphite, respectively (black: bare graphite, red: porous graphite). (c and d) XRD pattern and XPS C1s spectra of SiNWs-PG. In the XPS analysis, the deconvoluted peaks at 284.1, 284.8, and 285.1 eV indicates Si−C, C in graphite, and C−H bonding, respectively.

C−H bond, respectively. Considering a bonding of SiNWs-PG, XPS C1s result suggests that Si nanowires are chemically embedded in porous graphite, which is confirmed by the peak at 284.1 eV attributed to the Si−C bond (Figure 2d).[27] The element analysis showed that SiNWs-PG consists of 20 wt % silicon, 78.5 wt % carbon, and 1.5 wt % Au.

Considering a role of porous graphite as a buffer space for volume accommodation of the Si NWs porous graphite, the electrochemical performance of SiNWs-PG can be expected to be different from the directly Si nanowires grown on bare graphite (SiNWs-BG) without etching process (Figure S5). Both samples have 20 wt % silicon. Figure 3a exhibits the voltage profiles of bare graphite, porous graphite, SiNWs-BG, and SiNWs-PG at 0.05C between the voltage range of 0.005−1.4 V in lithium half-cells (2016R) (1C = 450 mA/cm^3 for bare and porous graphite, 1C = 1050 mA/cm^3 for SiNWs-BG and SiNWs-PG). The tests were performed in a comparable electrode density of 1.5 g/cm^3. As shown in Figure 3a (see Figure S6 for specific capacity plot), the first volumetric charge capacity based on porous graphite is 497 mAh/cm^3, of which value is slightly higher than bare graphite (441 mAh/cm^3). This higher capacity of the porous graphite than the bare one is due to the fact that lithium ion diffusion can be easily available through the edge plane rather than the basal plane of graphite after hydrogenation.[23] Also, SiNWs-PG exhibits a higher first charge (delithiation) capacity and Coulombic efficiency than SiNWs-BG, showing 1230 mAh/cm^3 and 91%, respectively, at 0.05C (SiNWs-BG shows 1005 mAh/cm^3 and 81%, respectively). The main reason for higher Coulombic efficiency of SiNWs-PG is believed to be related to that the Si NWs in the pores of graphite reduce side reactions with the electrolytes effectively related to SiNWs-BG. The volumetric charge capacity of SiNWs-PG shows 2.8 times greater than bare graphite, and the Coulomb efficiency is comparable to bare graphite (94%).
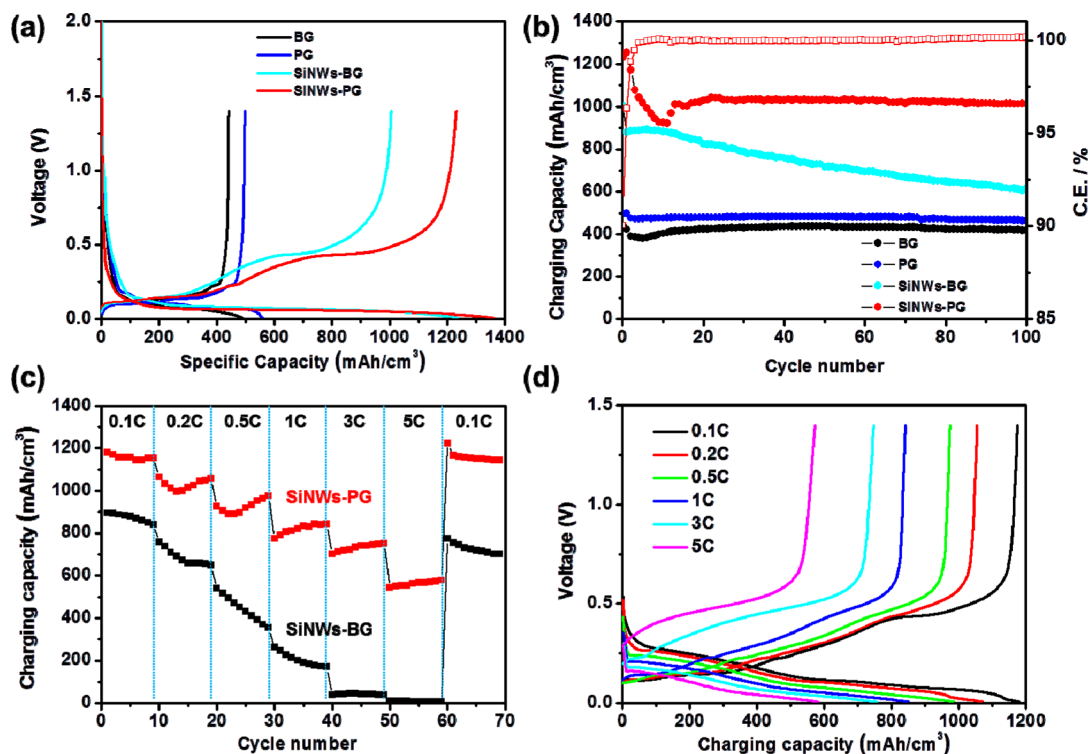
Figure 3. (a) Voltage profiles of bare graphite, porous graphite, SiNWs-BG, and SiNWs-PG at a 0.05C rate and (b) plot of volumetric charge (delithiation) capacity as a function of cycle number and Coulomb efficiency at 0.2C rate between 0.005 and 1.4 V in coin-type half-cell at 24 °C (1C = 450 mAh/cm^3 for bare graphite and porous graphite, 1C = 1050 mAh/cm^3 for SiNWs-BG and SiNWs-PG). (c) Rate capability of SiNWs-BG (black) and SiNWs-PG (red) with increasing C rate from 0.1 to 5C rate between 0.005 and 1.4 V in coin-type half-cell at 24 °C and (d) voltage profiles of (c) at each C rate (charge and discharge rates were same).

Figure 3b exhibits the cycle retention of each material at a 0.2C rate (also, see Figure S7 for the voltage profiles). Porous graphite shows 463 mAh/cm^3 and 93% retention after 100 cycles, while bare graphite shows 416 mAh/cm^3 and 94%. SiNWs-PG demonstrates little capacity fading after 100 cycles, showing a volumetric charge capacity of 1014 mAh/cm^3 and 100% coulomb efficiency (this performance is superior to that of SiNWs-BG). The initial capacity decreasing out to 10 cycles is originated from SEI formation on the exposure of the inner pore region.[28] Remarkably, without using a conducting agent (carbon black), the cycling stability of SiNWs-PG cycle is superior to chemically bridged Si/graphite composites,[20] blended SiNWs/graphite composites (15:85, w/w) including 20 wt % carbon black for electrode,[29] and comparable to physically bonded Si/B$_4$C/graphite composites with 40 wt % Si and 30 wt % conductive skeleton.[30]

Figure 3c demonstrates the excellent rate capability of SiNWs-PG compared to SiNWs-BG from 0.1C to 5C under conditions of same charge and discharge rates, respectively (1C = 1050 mA/cm^3) (for comparisons as a function of capacity, see Figures S6c and d). SiNWs-PG displays the charge capacities of 1057 mAh/cm^3, 843 mAh/cm^3, 751 mAh/cm^3, and 577 mAh/cm^3, respectively, at rates of 0.2, 1, 3, and 5C, respectively. The capacity retention at 5C is 49% capacity retention, while SiNWs-BG is ~0%. Based on the electrochemical performance of SiNWs-PG, the morphology maintenance and electrode of the sample after cycling is well-described to understand the reason for such excellent cycling stability and rate performance. The SEM image of SiNWs-PG confirmed the confinement of internally grown Si nanowires in the pores (Figure S8a and b), and the volume expansion of SiNWs-BG (Figure S8c and e) and SiNWs-PG electrodes (Figure S8d and f) were increased by 154% and 66% from the pristine electrodes with 26 and 29 μm, respectively. These results confirm that SiNWs-PG can maintain the interconnecting conductive network of the embedded Si nanowires in spite of without using conductive carbon additives which is required to deliver a high rate performance, resulting in the effective electron transport pathway. Overall, porous graphite contributes the structural integrity of Si nanowires.

In conclusion, Si nanowires grown in pores in etched graphite was successfully demonstrated as a new strategy with a high electrode density (1.5 g/cm^3) for an increasing volumetric capacity of the graphite. This strategy involved the graphite hydrogenation by Ni nanoparticles for porous structure, followed by Si nanowires growth inside porous graphite by VLS process after catalyst exchange. Especially, porous graphite as a template for Si nanowires played a key role of not only providing a free space to accommodate volume change of the internally grown Si nanowires during cycling, but also providing a good electron conducting pathway.

ASSOCIATED CONTENT

Ⓢ Supporting Information

Experimental methods; SEM images; battery cycling data; XRD data; TEM data. This material is available free of charge via the Internet at http://pubs.acs.org.

AUTHOR INFORMATION

Corresponding Author
*E-mail: spark@unist.ac.kr, jpcho@unist.ac.kr.

Notes
The authors declare no competing financial interest.

ACKNOWLEDGMENTS

REFERENCES

(1) Park, O. K.; Cho, Y.; Lee, S.; Yoo, H.-C.; Song, H.-K.; Cho, J. *Energy Environ. Sci.* **2011**, *4*, 1621.

(2) Choi, N.-S.; Chen, Z.; Freunberger, S. A.; Ji, X.; Sun, Y.-K.; Amine, K.; Yushin, G.; Nazar, L. F.; Cho, J.; Bruce, P. G. *Angew. Chem., Int. Ed.* **2012**, *51*, 9994.

(3) Note: Energy density (E) = $V \times It$ (Wh/kg), where V = the cell operating voltage (V), and It = the electrochemical capacity (Ah/kg) of the cell.

(4) Goodenough, J. B.; Kim, Y. *Chem. Mater.* **2009**, *22*, 587.

(5) Lee, K. T.; Jeong, S.; Cho, J. *Acc. Chem. Res.* **2013**, *46*, 1161.

(6) Liu, X. H.; Zhang, L. Q.; Zhong, L.; Liu, Y.; Zheng, H.; Wang, J. W.; Cho, J. H.; Dayeh, S. A.; Picraux, S. T.; Sullivan, J. P.; Mao, S. X.; Ye, Z. Z.; Huang, J. Y. *Nano Lett.* **2011**, *11*, 2251.

(7) Liu, X. H.; Zheng, H.; Zhong, L.; Huan, S.; Karki, K.; Zhang, L. Q.; Liu, Y.; Kushima, A.; Liang, W. T.; Wang, J. W.; Cho, J. H.; Epstein, E.; Dayeh, S. A.; Picraux, S. T.; Zhu, T.; Li, J.; Sullivan, J. P.; Cumings, J.; Wang, C. S.; Mao, S. X.; Ye, Z. Z.; Zhang, S. L.; Huang, J. Y. *Nano Lett.* **2011**, *11*, 3312.

(8) Liu, X. H.; Zhong, L.; Huang, S.; Mao, S. X.; Zhu, T.; Huang, J. Y. *ACS Nano* **2012**, *6*, 1522.

(9) Lee, S. W.; McDowell, M. T.; Choi, J. W.; Cui, Y. *Nano Lett.* **2011**, *11*, 3034.

(10) Kim, H.; Seo, M.; Park, M. H.; Cho, J. *Angew. Chem., Int. Ed.* **2010**, *49*, 2146.

(11) Liu, N.; Wu, H.; McDowell, M. T.; Yao, Y.; Wang, C.; Cui, Y. *Nano Lett.* **2012**, *12*, 3315.

(12) Jeong, H. M.; Lee, S. Y.; Shin, W. H.; Kwon, J. H.; Shakoor, A.; Hwang, T. H.; Kim, S. Y.; Kong, B.-S.; Seo, J.-S.; Lee, Y. M.; Kang, J. K.; Choi, J. W. *RSC Adv.* **2012**, *2*, 4311.

(13) Chan, C. K.; Peng, H. L.; Liu, G.; McIlwrath, K.; Zhang, X. F.; Huggins, R. A.; Cui, Y. *Nat. Nanotechnol.* **2008**, *3*, 31.

(14) Cui, L. F.; Yang, Y.; Hsu, C. M.; Cui, Y. *Nano Lett.* **2009**, *9*, 3370.

(15) Cho, J. *J. Mater Chem.* **2010**, *20*, 4009.

(16) Kim, H.; Han, B.; Choo, J.; Cho, J. *Angew. Chem., Int. Ed.* **2008**, *47*, 10151.

(17) Magasinski, A.; Dixon, P.; Hertzberg, B.; Kvit, A.; Ayala, J.; Yushin, G. *Nat. Mater.* **2010**, *9*, 353.

(18) Jo, Y. N.; Kim, Y.; Kim, J. S.; Song, J. H.; Kim, K. J.; Kwag, C. Y.; Lee, D. J.; Park, C. W.; Kim, Y. J. *J. Power Sources* **2010**, *195*, 6031.

(19) Kasavajjula, U.; Wang, C.; Appleby, A. J. *J. Power Sources* **2007**, *163*, 1003.

(20) Martin, C.; Alias, M.; Christien, F.; Crosnier, O.; Bélanger, D.; Brousse, T. *Adv. Mater.* **2009**, *21*, 4735.

(21) Lu, J. Q.; Yi, S. S. *Langmuir* **2006**, *22*, 3951.

(22) Campos, L. C.; Manfrinato, V. R.; Sanchez-Yamagishi, J. D.; Kong, J.; Jarillo-Herrero, P. *Nano Lett.* **2009**, *9*, 2600.

(23) van Schalkwijk, W.; Scrosati, B. *Advances in Lithium-Ion Batteries*; Kluwer Academic Publishers: Dordrecht, 2002; pp 27−29.

(24) ASM International Alloy Phase Diagram and the Handbook Committees. *ASM Handbook - Alloy Phase Diagrams*, Vol. 3; ASM International: Novelty, OH, 1992; p 1233.

(25) Yoshio, M.; Wang, H.; Fukuda, K. *Angew. Chem., Int. Ed.* **2003**, *42*, 4203.

(26) Ferrari, A. C.; Robertson, J. *Phys. Rev. B* **2000**, *61*, 14095.

(27) Liu, H.; Hamers, R. J. *Surf. Sci.* **1998**, *416*, 354.

(28) Deng, J.; Ji, H.; Yan, C.; Zhang, J.; Si, W.; Baunack, S.; Oswald, S.; Mei, Y.; Schmidt, O. G. *Angew. Chem., Int. Ed.* **2013**, *52*, 2326.

(29) Xu, W. L.; Flake, J. C. *J. Electrochem. Soc.* **2010**, *157*, A41.

(30) Chen, X.; Li, X.; Ding, F.; Xu, W.; Xiao, J.; Cao, Y.; Meduri, P.; Liu, J.; Graff, G. L.; Zhang, J.-G. *Nano Lett.* **2012**, *12*, 4124.